Supporting Information

Interfacial engineering of heterostructured CoTe@FeOOH nano-arrays with tailored d-band centers for electrocatalytic oxygen evolution

Jiangying Liu[a], Taotao Ai[a, *], Weiwei Bao[a, *], Jie Han[a], Junjun Zhang[b], Mameng Yang[a], Xueling Wei[a], Xiangyu Zou[a], Liangliang Feng [c, *]

[a]National & Local Joint Engineering Laboratory for Slag Comprehensive Utilization and Environmental Technology, School of Materials Science and Engineering, Shaanxi University of Technology, Hanzhong 723000, China.

[b]State Key Laboratory of High-efficiency Utilization of Coal and Green Chemical Engineering, College of Chemistry & Chemical Engineering, Ningxia University, Yinchuan 750021, Ningxia, P.R. China.

[c]School of Materials Science & Engineering, Shaanxi Key Laboratory of Green Preparation and Functionalization for Inorganic Materials, Shaanxi University of Science & Technology, Xi'an, Shaanxi 710021, China.

***Corresponding Author**

Taotao Ai, E-mail: aitaotao0116@126.com

Weiwei Bao, E-mail: baowei1834@163.com

Liangliang Feng, E-mail: fengll@sust.edu.cn

Number of pages: 20

Number of Figures: 10

Number of Tables: 2

List of Contents

1. Experimental Section

1.1 Materials

Iron chloride hexahydrate ($FeCl_3 \cdot 6H_2O$, 99%), sodium tellurite (Na_2TeO_3, 99%), iridium dioxide (IrO_2) and Nafion (5 wt%) were purchased from Aladdin Industrial Corporation. Ammonia water ($NH_3 \cdot H_2O$) comes from Macklin. Cobalt sulfate heptahydrate ($CoSO_4 \cdot 7H_2O$), sodium nitrate ($NaNO_3$) and hydrazine hydrate ($N_2H_4 \cdot H_2O$, 85%) were procured from Sinopharm chemical reagent co. Milli-Q ultrapure water was used for experiments. Nickel foam (NF) was used as the substrate. All these chemical reagents were used without any further purification.

1.2 Pretreated nickel foam

Nickel Foam (NF, 1×4 cm^2) needs to be pre-treated before use. NF is first ultrasonicated with 1.0 M hydrochloric acid solution for 30 minutes to remove the oxidized layer, and then ultrasonicated with ethanol and deionized water for 15 minutes in sequence, and then washed with alcohol and deionized water for several times and dried.

1.3 Synthesis of IrO_2 on NFs

5 mg of commercial IrO_2 powder was added to a solution containing 100 μL of ethanol, 80 μL of deionised water and 10 μL of Nafion, sonicated for half an hour, and then applied to a 1 cm^2 area of pre-treated NF and allowed to dry naturally in air.

1.4 General characterizations

XRD patterns were obtained on Rigaku Ultima IV Powder X-ray diffractometer with a Cu Kα X-ray source (λ = 0.15406 nm). Morphology of as-prepared catalysts was characterized by field-emission scanning electron microscope (FESEM, JSM-7610F, 15 kV). The morphologies of samples were further confirmed by transmission electron microscope (TEM, Titan3 G2 60-300, 300 kV). The elemental distributions of the

samples were characterized by the energy-dispersive X-ray spectroscopy (EDS) mapping affiliated to the STEM, and the EDS was also imaged from the STEM. Raman spectra were collected by Raman spectrometer (LabRAM HR JYEvolution) with 532 nm of green laser. A Thermo Fisher Scientific K-Alpha was performed to get the X-ray photoelectron spectroscopy (XPS) data, using a monochromated source of X-rays (Mg K_{α}, photon energy 1253.6 eV) for excitation.

1.5 Electrochemical measurements

All electrochemical tests were carried out in a standard three-electrode system by means of a CHI660E electrochemical bench (CH Instruments, Shanghai) at room temperature. Specifically, a mercuric oxide electrode (Hg/HgO) electrode, a graphite-carbon rod electrode, and a prepared catalyst electrode were used as the reference, counter, and working electrodes, respectively. All electrochemical measurements were performed in 1 M KOH solution. The measured potentials were converted to reversible hydrogen electrode (RHE) according to the formula: $E_{RHE} = E_{Hg/HgO} + 0.0591 \times pH + 0.098$. The pH value of 1.0 M KOH was 13.78. The geometrical area of all the samples was controlled to be 1 cm^2. The scan rate was 5 mV s^{-1}, and all the results were calibrated using IR compensation. EIS curves were obtained for an amplitude of 5 mV over an open-circuit potential range of 0.01~100 kHz.

The ECSA-normalized current density for as-prepared catalysts was calculated by:

$$\text{ECSA-normalized current density} = \text{current density} \times C_s/C_{dl}$$

where C_s is the specific capacitance. In this work, 0.04 mF cm^{-2} was adopted as the value of C_s based on previously reported OER catalysts in alkaline solution.

1.6 Computational methodology

In order to understand the origin of highly boosted OER performance of CoTe@FeOOH, the density functional theory (DFT) calculations were carried out by

using the Vienna ab-initio simulation package (VASP) code. Calculations were performed using a planar fluctuation energy cutoff energy set to 450 eV and a 2 × 2 × 1 Monkhorst-Pack k-point sampling was chosen to obtain well-converged energy values. All structures were fully optimized with a force tolerance of 0.01 eV $Å^{-1}$. In addition, a vacuum plate with a thickness of 15 Å was added to prevent interactions between the plates. The energy profiles of the OER process were calculated based on the following mechanism:

(I) $OH^- + * \rightarrow OH^* + e^-$

(II) $OH^* + OH^- \rightarrow O^* + H_2O + e^-$

(III) $O^* + OH^- \rightarrow OOH^* + e^-$

(IV) $OOH^* + OH^- \rightarrow O_2 + H_2O + * + e^-$

The reaction-free energy of these elementary steps was calculated following the scheme described in previous theoretical studies of OER.

The overpotential was defined as:

$$\eta = \max(\Delta G_I, \Delta G_{II}, \Delta G_{III}, \Delta G_{IV}) - 1.23 \text{ eV}$$

2. Supplementary Figures

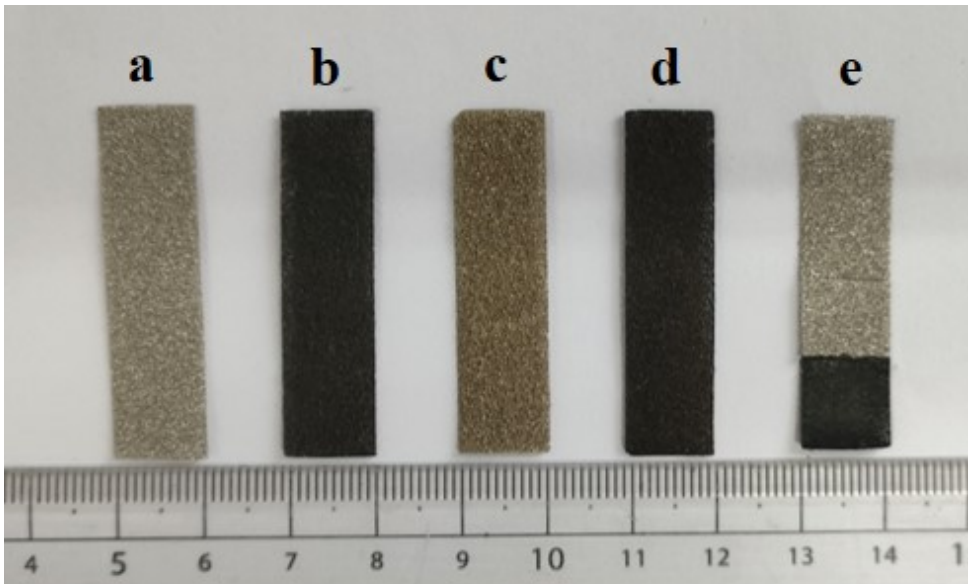

Figure S1. Optical image of (a) bare NF, (b) CoTe/NF, (c) FeOOH/NF, (d) CoTe@FeOOH/NF, and (e) IrO_2/NF, respectively.

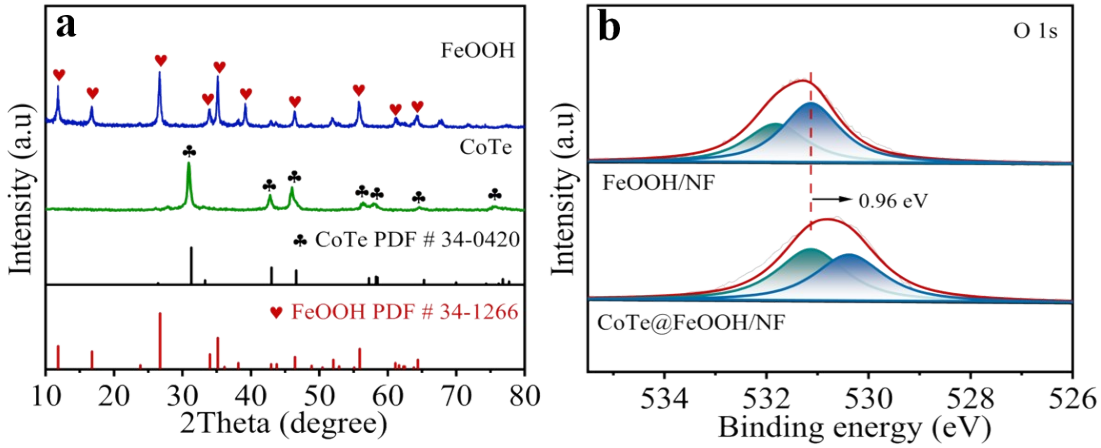

Figure S2. (a) XRD patterns of CoTe powder and FeOOH powder. (b) High-resolution XPS spectra of O 1s for different samples.

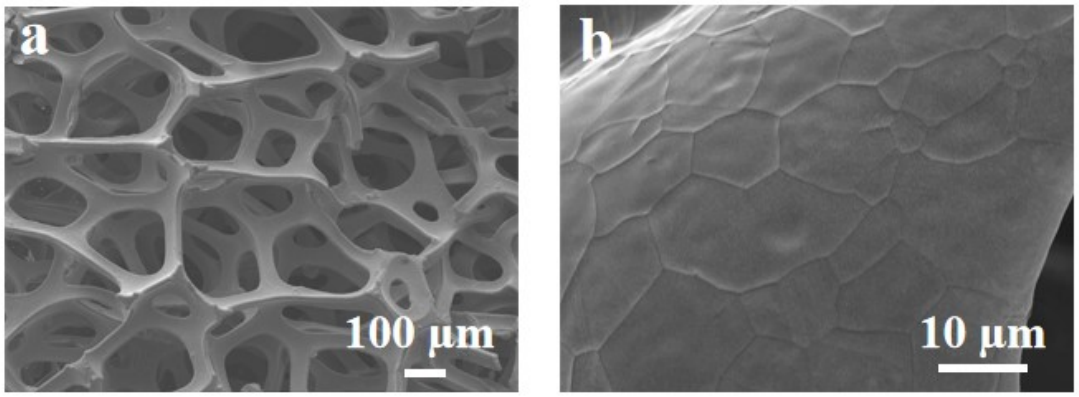

Figure S3. The SEM images of bare NF (a) with low-magnification, (b) with high-magnification.

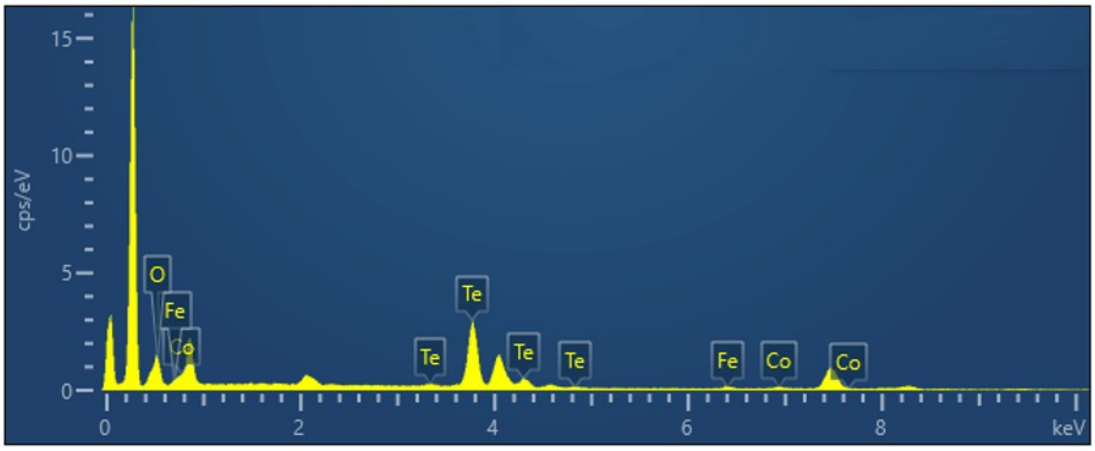

Figure S4. Energy dispersive spectroscopy (EDS) spectrum of CoTe@FeOOH/NF.

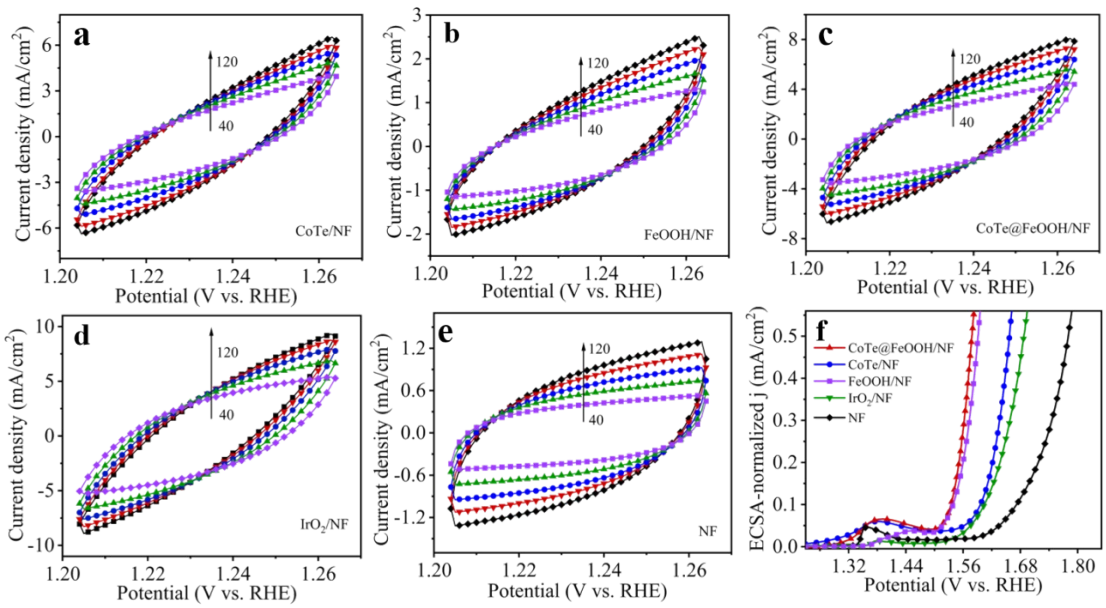

Figure S5. Cyclic voltammograms at different scan rates (from 40 mV s^{-1} to 120 mV s^{-1} with an interval rate of 20 mV s^{-1}) of (a) CoTe/NF, (b) FeOOH/NF, (c) CoTe@FeOOH/NF, (d) IrO_2/NF, and (e) NF. (f) ECSA-normalized LSV curves.

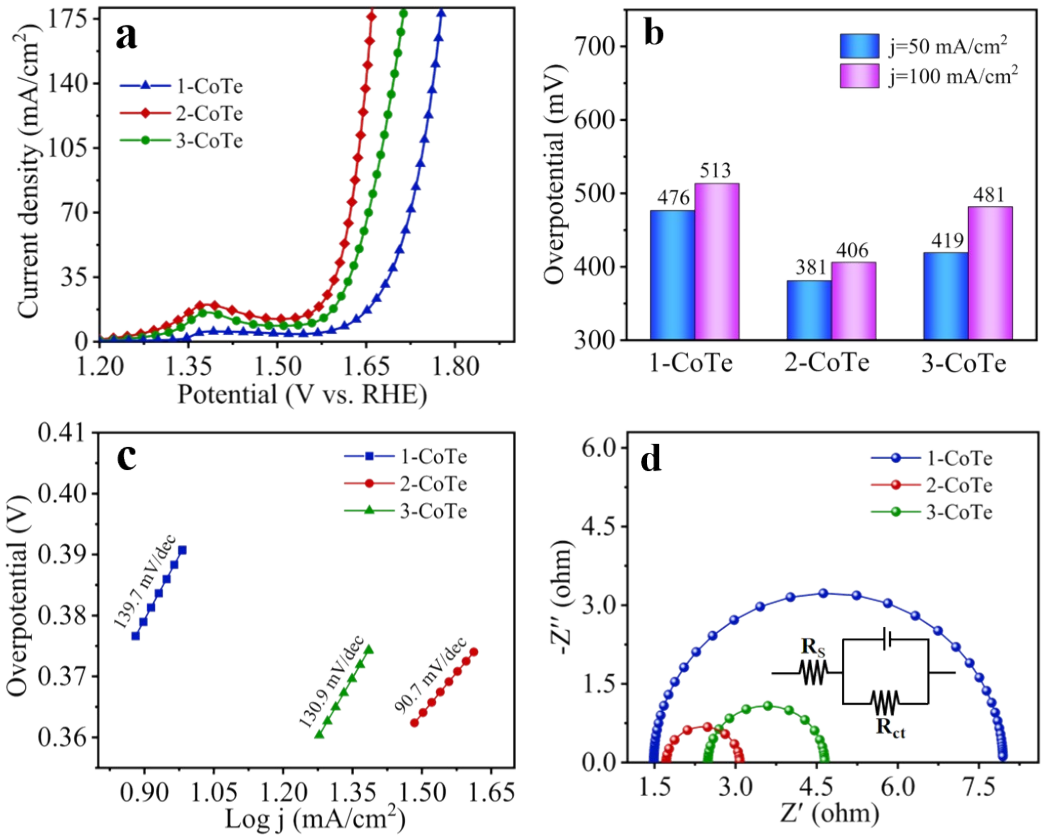

Figure S6. OER property of 1-CoTe, 2-CoTe, and 3-CoTe. (a) IR-compensated LSV curves, (b) overpotentials, (c) Tafel slopes, (d) the Nyquist plots from 10 kHz to 0.01 Hz.

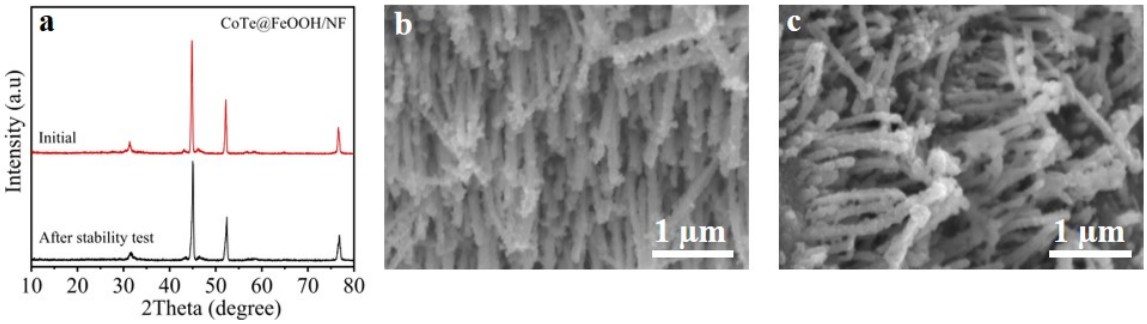

Figure S7. (a) XRD patterns of CoTe@FeOOH/NF before and after stability test. SEM image of CoTe@FeOOH/NF before and after stability test, (b) before, (c) after stability test.

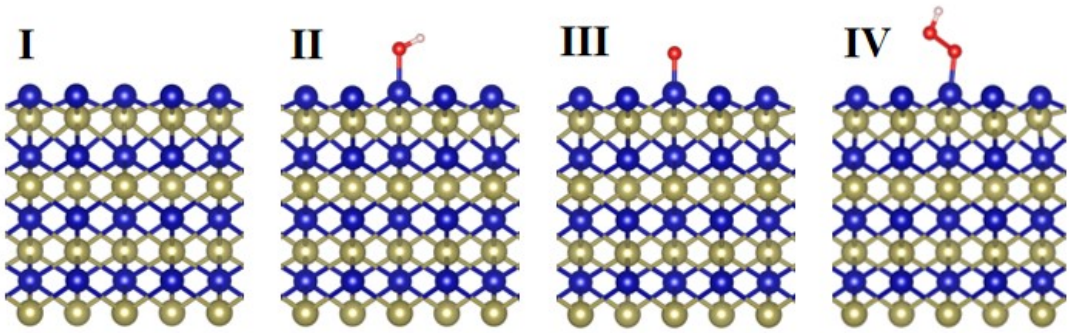

Figure S8. Models of adsorbed OER intermediates for CoTe.

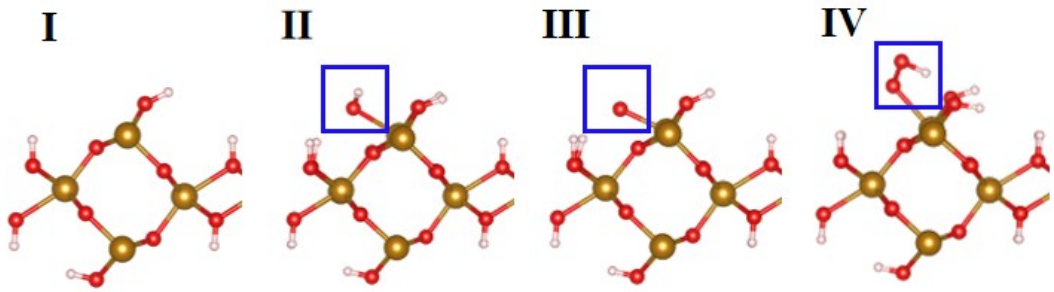

Figure S9. Models of adsorbed OER intermediates for FeOOH.

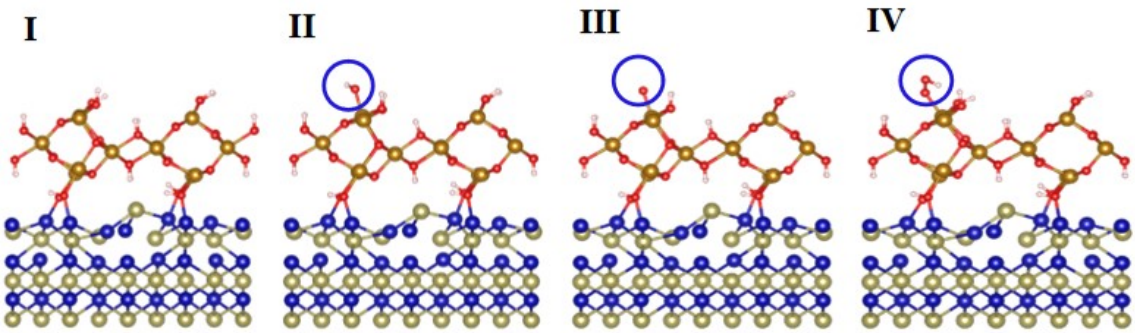

Figure S10. Models of adsorbed OER intermediates for CoTe@FeOOH.

3. Supplemental Tables

Table S1. Comparison of OER activity of CoTe@FeOOH/NF with other reported non-precious metal-based electrocatalysts in alkaline medium (1 M KOH).

Catalysts	Current density ($mA\ cm^{-2}$)	Overpotential (mV)	Reference
CoTe@FeOOH/NF	50	308	This work
CoTe@FeOOH/NF	100	325	
CoTeNR/NF	100	350	1
$CoTe_2$	10	357	2
CoTe	10	365	
$Ni_2(OH)_2CO_3$	10	404	3
Co-NiSe/NF	100	380	4
CoNi LDH@Te	10	360	5
NiTe/NiCo-LDH	100	376	6
CoS-$Co(OH)_2$@aMoS_{2+x}/NF	10	380	7
NiFe LDH/NC	10	330	8
NiFe LDH/NC	20	375	
$P_{1.0}$-MoS_2/Ni_3S_2/NF	100	435	9
$Ni_{66}Fe_{34}$-NC	10	467	10
Fe-CoOOH/G	10	330	11
Fe-CoOOH/G	50	408	
Co/CoTe	50	400	12

Table S2. OER features of presented catalysts.

Catalyst	Calculated from CV	
	Double Layer Capacitance (C_{dl})/mF cm^{-2}	**Electyochemically active surface area (ECSA)/cm^2**
CoTe@FeOOH/NF	16.43	410.75
CoTe/NF	10.2	255
FeOOH/NF	6.35	158.75
IrO_2/NF	9.74	243.5
NF	5.63	140.75

4. Notes and references

1 L. Yang, H. X. Xu, H. B. Liu, D. C. Cheng and D. P. Cao, Active Site Identification and Evaluation Criteria of In Situ Grown CoTe and NiTe Nanoarrays for Hydrogen Evolution and Oxygen Evolution Reactions, *Small Methods.*, 2019, **3**, 1900113-1900123.

2 Q. Gao, C. Q. Huang, Y. M. Ju, M. R. Gao, J. W. Liu, D. An, C. H. Cui, Y. R. Zheng, W. X. Li and S. H. Yu, Phase-selective syntheses of cobalt telluride nanofleeces for efficient oxygen evolution catalysts, *Angew. Chem. Int. Ed.*, 2017, **56**, 7769-7773.

3 W. J. Zhu, G. X. Zhu, J. Hu, Y. Zhu, H. Chen, C. L. Yao, Z. X. Pi, S. W. Zhu and E. Li, Poorly crystallized nickel hydroxide carbonate loading with Fe^{3+} ions as improved electrocatalysts for oxygen evolution, *Inorg Chem Commun.*, 2020, **114**, 107851.

4 D. X. Liang, J. X. Mao, P. Liu, J. W. Li, J. Y. Yan, and W. B. Song, In-situ doping of Co in nickel selenide nanoflower for robust electrocatalysis towards oxygen evolution, *Int. J. Hydrog.*, 2020, **45**, 27047-27055.

5 Y. Qi, Z. Yang, Y. C. Dong, X. Q. Bao, J. L. Bai, H. Li, M. T. Wang and D. H. Xiong, A CoNi telluride heterostructure supported on Ni foam as an efficient electrocatalyst for the oxygen evolution reaction, *Inorg. Chem. Front.*, 2022, **9**, 5240-5251.

6 B. He, P. Zhao, G. X. Pan, Q. Lu, H. Q. Li, F. Ye, Y. W. Tang, Q. L. Hao and Z. Su, Interface engineering of NiTe/NiCo-LDH core-shell structure to enhance oxygen evolution electrocatalysis performance, *J. Alloys Compd.*, 2023, **938**, 168673.

7 T. Yoon K. S. Kim, Water Splitting: One-Step Synthesis of CoS-Doped β-$Co(OH)_2$@ Amorphous MoS_{2+x} Hybrid Catalyst Grown on Nickel Foam for High-

Performance Electrochemical Overall Water Splitting, *Adv. Funct. Mater.*, 2016, **26**, 7386-7393.

8 C. Tang, H. S. Wang, H. F. Wang, Q. Zhang, G. L. Tian, J. Q. Nie, F. Wei, Spatially confined hybridization of nanometer-sized NiFe hydroxides into nitrogen-doped graphene frameworks leading to superior oxygen evolution reactivity, *Adv. Mater.*, 2015, **27**, 4516-4522.

9 Y. Y. Miao, S. F. Yuan, H. Ren, A. Addad, A. Barras, P. Roussel, M. A. Amin, S. Szunerits and R. Boukherroub, Interface Engineering of an Ultrathin Hierarchical Phosphorus-Doped MoS_2/Ni_3S_2 Heterostructure on Nickel Foam for Efficient Water Splitting, *ACS Appl. Energy Mater.*, 2023, **6**, 5856-5867.

10 M. Ma, A. Kumar, D. Wang, Y. Wang, Y. Jia, Y. Zhang, G. X. Zhang, Z. F. Yan and X. M. Sun, Boosting the bifunctional oxygen electrocatalytic performance of atomically dispersed Fe site via atomic Ni neighboring, *Appl. Catal. B.*, 2020, **274**, 119091.

11 X. T. Han, C. Yu, S. Zhou, C. T. Zhao, H. W. Huang, J. Yang, Z. B. Liu, J. J. Zhao, and J. S. Qiu, Ultrasensitive iron-triggered nanosized Fe-CoOOH integrated with graphene for highly efficient oxygen evolution, *Adv. Energy Mater.,* 2017, **7**, 1602148.

12 R. Yoo, K. Min, H. Kim, D. Lim and S. H. Baeck, Prussian blue analog-derived Co/CoTe microcube as a highly efficient and stable electrocatalyst toward oxygen evolution reaction, *Appl. Surf. Sci.*, 2022, **581**, 152405.